Biogeosciences Discuss., 8, 10155–10185, 2011
www.biogeosciences-discuss.net/8/10155/2011/
doi:10.5194/bgd-8-10155-2011

Biogeosciences Discussions

Processes controlling the Si-isotopic composition in the Southern Ocean and application for paleoceanography

F. Fripiat[1,2], A.-J. Cavagna[3], F. Dehairs[3], A. de Brauwere[3,4], L. André[1], and D. Cardinal[1,*]

[1]Section of Mineralogy and Petrography, Royal Museum for Central Africa, Tervuren, Belgium
[2]Department of Earth and Environmental Sciences, Université Libre de Bruxelles, Brussels, Belgium
[3]Analytical and Environmental Chemistry & Earth System Sciences, Vrije Universiteit Brussel, Brussels, Belgium
[4]Institute of Mechanics, Materials and Civil Engineering (IMMC), Université Catholique de Louvain, Louvain-la-Neuve, Belgium
[*]now at: Laboratoire d'Océanographie et du Climat: Expérimentations et Approches Numériques (LOCEAN), Université Pierre et Marie Curie, Paris, France

Received: 8 September 2011 – Accepted: 29 September 2011 – Published: 17 October 2011

Correspondence to: F. Fripiat (ffripiat@ulb.ac.be)

Published by Copernicus Publications on behalf of the European Geosciences Union.

Abstract

Southern Ocean biogeochemical processes have an impact on global marine primary production and global elemental cycling, e.g. by likely controlling glacial-interglacial pCO_2 variation. The natural silicon isotopic composition (δ^{30}Si) of sedimentary biogenic silica has been used to reconstruct past Si-consumption:supply ratio in the surface waters. We present a new dataset in the Southern Ocean which includes for the first time summer δ^{30}Si signatures of suspended biogenic silica (i) for the whole water column at three stations and (ii) in the mixed layer at seven stations from the sub-tropical zone up to the Weddell Gyre.

In general, the biogenic silica isotopic composition at depth reflected a mixed layer origin and seemed not affected by any diagenetic effect in the water column, even if in the northern part of the Weddell Gyre an effect of biogenic silica dissolution cannot be ruled out.

We develop a mechanistic understanding of the processes involved in the modern Si-isotopic balance, by implementing a mixed layer model. We observe that the accumulated biogenic silica (sensu Rayleigh) should satisfactorily describe the δ^{30}Si composition of biogenic silica exported out of the mixed layer, within the limit of the current analytical precision on the δ^{30}Si. The failures of previous models (Rayleigh and steady state) become apparent especially at the end of the productive period in the mixed layer, when biogenic silica production is low. This results from: (1) a higher biogenic silica dissolution:production ratio imposing a lower net fractionation factor and (2) a higher Si-supply:Si-uptake ratio supplying light Si-isotopes into the mixed layer. The latter effect is especially expressed when the summer mixed layer becomes strongly Si-depleted together with a large vertical silicic acid gradient.

1 Introduction

In the Southern Ocean, the deep nutrient-rich waters ascend into the surface layer south of the Polar Front (PF) and are returned to the subsurface northward before the available pools of nitrogen and phosphorus are fully used by phytoplankton. In contrast, silicic acid ($Si[OH]_4$) becomes strongly depleted by diatom growth (Sarmiento et al., 2004). The balance between the efficiency of the biological pump (e.g. its ability to strip nutrients out of the mixed layer) and deep ocean ventilation releasing CO_2, are both likely to control the atmospheric CO_2 concentrations on glacial/interglacial timescales (Anderson et al., 2002, 2009; Brzezinski et al., 2002; Sigman et al., 2010).

The $\delta^{30}Si$ signatures of biogenic silica ($= {}^{30}R_{bSiO2}:{}^{30}R_{standard} - 1$, reported in permil units, ‰, where ${}^{30}R = {}^{30}Si:{}^{28}Si$), provide a view of Si-nutrient utilization in paleoceanography, and have been used to formulate and test hypotheses on both Southern Ocean productivity and fluctuations in atmospheric pCO_2 over glacial cycles (De La Rocha et al., 1998; Anderson et al., 2002; Brzezinski et al., 2002; De La Rocha, 2006; Beucher et al., 2007). During silicic acid consumption by diatoms, the lighter Si isotope (^{28}Si) is preferentially consumed, leaving the silicic acid pool enriched in heavy Si-isotopes (^{30}Si) (De La Rocha et al., 1997). Such preferential incorporation of ^{28}Si into biogenic silica ($bSiO_2$) is defined by a fractionation factor (${}^{30}\varepsilon$), which is equivalent to the ratio of the reaction rates of the heavy (^{30}k) and light (^{28}k) Si-isotopes ($= {}^{30}k:{}^{28}k - 1$, reported in permil units, ‰). Therefore, for a given set of conditions setting the supply of $Si(OH)_4$, a relationship is expected between the decrease of $Si(OH)_4$ concentration due to the Si-uptake and the increase of $\delta^{30}Si$ of both $bSiO_2$ and $Si(OH)_4$ (De La Rocha et al., 1997). However, the complete calibration of this proxy in the modern ocean has still not be fully achieved and processes such as mixing and $bSiO_2$ dissolution can bias the expected relationship between $Si(OH)_4$ concentration and $\delta^{30}Si$ composition (Demarest et al., 2009). For example, contemporary isotopic compositions of biogenic silica vary widely in the Southern Ocean (−0.5 to +2.5 ‰), while variations of silicic acid is less (from +1.5 to 3.4 ‰) (Varela et al., 2004; Cardinal et al., 2005, 2007; Fripiat et al., 2011b; Cavagna et al., 2011b). None of the existing isotopic fractionation models are capable of reproducing these differences. This highlights the significant importance of fully understanding the different processes involved in contemporary Si-isotopic balances before applying this proxy to reconstruct past ocean environments.

New data from the summer Antarctic Circumpolar Current (ACC) are presented here, looking at the relationship between $\delta^{30}Si_{Si(OH)4}$ and $\delta^{30}Si_{bSiO2}$ in the mixed layer. Primary objectives are to (1) assess the processes controlling mixed layer $\delta^{30}Si_{bSiO2}$ and across the water column, and (2) the impact of such processes on the relationship between the relative silicic acid utilisation and $\delta^{30}Si$.

2 Materials and methods

2.1 Sampling and hydrology

Between 8 February and 8 March 2008, the International Polar Year (IPY) BONUS-GoodHope (BGH) cruise aboard R/V *Marion Dufresne* covered a transect from Cape Basin to the north of the Weddell Gyre (up to 58° S) centred around the 0° meridian (Fig. 1). Biogenic silica was sampled (1) in the mixed layer at 7 stations crossing the different hydrographic regimes of the ACC, and (2) from a profile of the surface to the deep ocean at 3 stations. For these stations and others from the same cruise, the water column profiles of silicic acid $\delta^{30}Si$ are discussed in an associated paper (Fripiat et al., 2011a).

Seawater was collected using a CTD Rosette equipped with 12 l Niskin bottles. Water samples (~0.25 to ~10 l) were immediately filtered on 0.4 µm Nuclepore polycarbonate membranes, using Perspex filtration units under the pressure of filtered air (0.4 µm Nuclepore). Filtered water samples for silicic acid analyses, were stored in acid-cleaned polypropylene (PP) bottles at room temperature in the dark. Nuclepore membranes were stored in polycarbonate Petri dishes and dried overnight at 50 °C. Large Volume Filtration Systems, hereafter referred to as “in situ pumps” (Challenger

Oceanic Systems and Services, Surry, UK) sampled the complete water column by filtering 15 to 250 l of water through hydrophylic polyesthersufone membranes (SUPOR, 293 mm Ø, 0.43 µm). After partitioning the filters amongst the different end-users knowing the used filter surface, the pieces of SUPOR membranes were dried overnight at 50 °C and stored in Petri dishes in the dark at ambient temperature.

2.2 Analyses

Samples were processed at land-based laboratory (RMCA, Tervuren). For $bSiO_2$ the membranes were submitted to a wet-alkaline digestion (adapted from Ragueneau et al., 2005) whereby $bSiO_2$ is dissolved with a 0.2 µmol l^{-1} NaOH solution (pH 13.3) at 100 °C for 40 min. As this digestion can also dissolve some lithogenic silica, we also analyzed aluminum (Al) in the digested solution to check for possible lithogenic contamination. Al in digested samples has been measured with a Sector Field Inductively Coupled Plasma Mass Spectrometer (SF-ICP-MS Element2, detection limit = 0.01 ppm). Using a Si:Al mass ratio of 3.74 for average crust (Taylor and McLennan, 1985), the lithogenic silica contributed to less than 2.5 % of the Si in digested samples. The distribution of clays in marine sediments along the BONUS-GoodHope transect is: <10 % kaolinite, >40 % illite, <20 % smectite and 20–30 % chlorite (Fütterer, 2006). The δ^{30}Si signatures for these different clays published in previous studies are the following: kaolinite -2.2 ± 0.4 ‰ (Ziegler et al., 2005; Opfergelt et al., 2010); illite: -0.9 ± 0.2 ‰ (Douthitt, 1982) smectite: -0.3 ± 0.2 ‰ (Georg et al., 2009). No δ^{30}Si value is available for chlorite. Setting the chlorite δ^{30}Si values to the one of kaolinite which maximizes the potential clay δ^{30}Si contamination, we estimate an average clay δ^{30}Si value for the BONUS-GoodHope transect of -1.3 to -1.0 ‰ using mass and isotopic balances from the expected distribution of clays. Taking the heavier BGH $\delta^{30}Si_{bSiO2}$ and the calculated clay δ^{30}Si, with a lithogenic silica contamination of 2.5 %, the maximum potential contribution of such lithogenic Si to the measured δ^{30}Si is 0.1 ‰. Such contribution can be neglected since it is similar to the achieved analytical precision for δ^{30}Si (Abraham et al., 2008).

$Si(OH)_4$ and $bSiO_2$ concentrations were determined via a colorimetric method (Grasshoff et al., 1983) on the same samples as for Si-isotopic composition. Since $Si(OH)_4$ concentrations of surface and some subsurface samples at stations north of the Polar Front (PF) were too low (<10 µmol l^{-1}) to directly apply the Si purification procedure required for Si-isotopic measurement (De La Rocha et al., 1996), a $Si(OH)_4$ preconcentration step was performed. It was achieved using a protocol adapted by Brzezinski et al. (2003) and Reynolds et al. (2006) from the MAGIC method (Karl and Tien, 1992). Briefly, the method consists of one or two steps (depending of the Si-recovery of the first step) of the co-precipitation of $Si(OH)_4$ with brucite ($Mg(OH)_2$), by increasing pH either with NaOH 1 µmol l^{-1} (20 ml l^{-1} seawater (Reynolds et al., 2006)) or NH_4OH 13.5 µmol l^{-1} (6 ml l^{-1} seawater (Brzezinski et al., 2003)). The precipitates were recovered by centrifugation and then redissolved with HCl.

Silicon was co-precipitated with triethylamine molybdate (De La Rocha et al., 1996) with a minimum Si requirement of ~1.5 µmol Si. After combustion of the silicomolybdate precipitate in covered Pt crucibles at 1000 °C, the pure cristobalite phase was transferred to pre-cleaned polypropylene vials. Dissolution of cristobalite was done in a dilute HF/HCl mixture as described in Cardinal et al. (2003). Isotopic measurements were carried out on a Nu Plasma MC-ICP-MS (ULB, Brussels) using Mg external doping in dry plasma mode following Abraham et al. (2008). The average precision and reproducibility of the measurements are ±0.1 ‰ (±1 sd) for δ^{30}Si (Reynolds et al., 2007). The accuracy of the measurements is checked on a daily basis on secondary reference materials (e.g. Diatomite) with known Si isotopic compositions resulting from an inter-comparison exercise (Reynolds et al., 2007).

3 Results

Surface $\delta^{30}Si_{Si(OH)4}$ and $[Si(OH)_4]$ display an opposite pattern with latitude (Table 1 and Fig. 2a). There is a ^{30}Si enrichment associated with the northward decreasing $Si(OH)_4$

gradient across the Polar Front (PF) as has been observed earlier for $\delta^{30}Si_{Si(OH)4}$ (Varela et al., 2004; Cardinal et al., 2005) and $Si(OH)_4$ concentrations (Brzezinski et al., 2001; Quéguiner and Brzezinski, 2002). $\delta^{30}Si_{bSiO2}$ values are systematically lighter than $\delta^{30}Si_{Si(OH)4}$ values in agreement with the preferential uptake of ^{28}Si by diatoms. From the WG to the PFZ we observe a trend of increasing $\delta^{30}Si_{bSiO2}$ following the $\delta^{30}Si_{Si(OH)4}$ gradient, although the trend is much steeper for the former, as also observed by Varela et al. (2004) and Cardinal et al. (2007). North of the PFZ and SAZ, respectively, the $\delta^{30}Si_{bSiO2}$ and $\delta^{30}Si_{Si(OH)4}$ trend reverses, again displaying a steeper gradient for $\delta^{30}Si_{bSiO2}$values. This decoupling is reflected in the apparent fractionation factor ($\Delta^{30}Si = \delta^{30}Si_{Si(OH)4} - \delta^{30}Si_{bSiO2}$) which varies widely with latitude (Fig. 2b). Low $\Delta^{30}Si$ values ($\sim 0.35 \pm 0.10$ ‰) are observed at the PF and in the PFZ. Such low values seem to be a recurrent feature in the Southern Antarctic Circumpolar Current at low $Si(OH)_4$ concentrations (Fig. 3). The mixed layer BONUS-GoodHope results for $\delta^{30}Si_{Si(OH)4}$ (+1.8 to +3.2 ‰) and for $\delta^{30}Si_{bSiO2}$ (+0.3 to +2.5 ‰) fall in the range reported for previous Southern Ocean studies (+1.5 to +3.1 ‰; for $\delta^{30}Si_{Si(OH)4}$; −0.5 to +2.6 ‰ for $\delta^{30}Si_{bSiO2}$) (Varela et al., 2004; Cardinal et al., 2005, 2007; Fripiat et al., 2011b; Cavagna et al., 2011b). For $bSiO_2$, the previous studies are restricted to the Seasonal Ice Zone (SIZ), AZ, and PFZ. However, it is interesting to note that the range of $\delta^{30}Si_{bSiO2}$ values are roughly two times those of $\delta^{30}Si_{Si(OH)4}$ (Fig. 3a).

The water column profiles of $Si(OH)_4$ and $\delta^{30}Si_{Si(OH)4}$ clearly display ^{30}Si enrichment and $Si(OH)_4$ depletion towards the surface (Table 1; Fripiat et al., 2011a), similar to previous studies (e.g. Cardinal et al., 2005). While biogenic silica concentrations exhibit an inverse pattern (Fig. 4a). $\delta^{30}Si_{bSiO2}$ remains constant with depth in the AZ and in the upper ~1000 m of the northern WG and the PFZ (Fig. 4b). In the WG $\delta^{30}Si_{bSiO2}$ decreases just below the mixed layer, coinciding with a decrease in $bSiO_2$ and $\delta^{30}Si_{Si(OH)4}$, while below 1000 m $\delta^{30}Si_{bSiO2}$ increases.

4 Discussion

Proxies can be influenced by multiple factors, and the sensitivity of a specific proxy to these factors likely changes in space and time. In the following sections, we discuss the processes controlling the origin of the isotopic composition of biogenic silica in the mixed layer (Sect. 4.1.) and subsequently the fate of the isotopic composition of biogenic silica across the water column (Sect. 4.2.).

4.1 Origin of the mixed layer biogenic silica isotopic composition

Two models are commonly applied to describe Si-isotopic fractionation during Si-consumption by diatoms in the mixed layer, directly linking the $\delta^{30}Si$ to the relative utilisation of $Si(OH)_4$. If a pool of silicic acid is consumed without resupply during the consumption process, then the isotopic evolution of the remaining $Si(OH)_4$, instantaneous $bSiO_2$ (hereafter referred to with the superscript "inst"), and accumulated $bSiO_2$ (hereafter referred to with the superscript "acc") should follow the Rayleigh fractionation equations (De La Rocha et al., 1997):

$$\delta^{30}Si_{Si(OH)4_{[t]}} = \delta^{30}Si_{Si(OH)4_{[t0]}} + {}^{30}\varepsilon \cdot \ln(f) \quad (1)$$

$$\delta^{30}Si^{Inst}_{bSiO2[t]} = \delta^{30}Si_{Si(OH)4[t]} + {}^{30}\varepsilon \quad (2)$$

$$\delta^{30}Si^{acc}_{bSiO2[t]} = \delta^{30}Si_{Si(OH)4_{[t0]}} - {}^{30}\varepsilon \cdot \frac{f \cdot \ln(f)}{1-f} \quad (3)$$

where f is the $[Si(OH)_4]_{[t]}$: $[Si(OH)_4]_{[t0]}$ ratio. The subscript "$[t]$" is the sampling time and "$[t0]$" the initial time. The alternative to this closed system is the open, flow-through system, where the substrate is continuously supplied to the place where the reaction continuously occurs in the same extent (also referred to as steady state system, Fry, 2006).

$$\delta^{30}Si_{Si(OH)4_{[t]}} = \delta^{30}Si_{Si(OH)4_{[t0]}} - {}^{30}\varepsilon \cdot (1-f) \quad (4)$$

$$\delta^{30}Si_{bSiO2[t]} = \delta^{30}Si_{Si(OH)4[t0]} - {}^{30}\varepsilon \cdot f = \delta^{30}Si_{Si(OH)4[t]} + {}^{30}\varepsilon \quad (5)$$

The steady state system assumes equilibrium and does not represent a temporal evolution. Conceptually for the Southern Ocean, this poses a problem, since Si-depletion is observed in the mixed layer as a result of varying the growth and export of diatoms (Brzezinski et al., 2001).

Neither of these models can explain the large variability that is observed in $\delta^{30}Si_{bSiO2}$ values compared to $\delta^{30}Si_{Si(OH)4}$ (Fig. 3a), and therefore the associated low and high $\Delta^{30}Si$ ($\Delta^{30}Si = \delta^{30}Si_{bSiO2} - \delta^{30}Si_{Si(OH)4}$; Fig. 3b). Below, a box model writing conservation of Si mass and isotopic composition along the productive period for the mixed layer is implemented.

4.1.1 Model description

Figure 5a shows the model structure with the associated fluxes: $Si(OH)_4$ supply, $bSiO_2$ production, dissolution, and export. The box represent a 100 m deep mixed layer and has two compartments: the $Si(OH)_4$ and $bSiO_2$ pools. The accumulated exported $bSiO_2$ is also simulated, to assess the effects of seasonal changes upon the isotopic composition of exported $\delta^{30}Si_{bSiO2}$, i.e. the variable measured in paleoceanography. Here, the productive period is assumed to have a duration of 90 days, with the productive peak roughly centered in December, as shown by chl-*a*/POC satellite data and modeling studies (Pondaven et al., 1998; Moore and Abbot, 2000; Allison et al., 2010). Across the BGH transect which took place in late summer 2008, mixed layers silicon properties can be considered as representative of final summer conditions. This is supported by Si-uptake in the mixed layer being in the lower range of published values, 0.02 ± 0.03 µmol Si l^{-1} d^{-1} (mean Si-uptake from ^{30}Si tracer incubations for the BGH transect, $n = 27$ triplicates; Fripiat, 2010). This indicates that the end of the growth period has been reached. The PFZ station was chosen as a case study for this simulation as both (1) near complete Si-depletion (Fig. 2a) and (2) low $\Delta^{30}Si$ are observed (Fig. 2b). The model initial conditions (i.e. before the start of the growth season) as

set using the Si-characteristics of subsurface waters defined for the PFZ in Fripiat et al. (2011a; $[Si(OH)_4] = 15 \pm 11$ µmol l^{-1}; $\delta^{30}Si_{Si(OH)4} = 1.91 \pm 0.24$ ‰), argued here to represent the winter mixed layer.

The vertical supply of Si to the mixed layer is described either by a constant flux (zero order equation) or by 10 discrete mixing events (every 9 days) supplying an equal quantity of Si into the mixed layer. The gross uptake rate of Si (= gross $bSiO_2$ production) during the growth period is described by a Michaelis-Menten saturation function:

$$V_{Si[t]} = \frac{V_{max} \cdot [Si(OH)_4]}{k_{Si} + [Si(OH)_4]} \quad (6)$$

where V_{Si} is the specific uptake rate (d^{-1}), V_{max} (d^{-1}) the maximum specific uptake rate, and k_{Si} (µmol l^{-1}) the $Si(OH)_4$ concentration when $V_{Si} = V_{max}/2$. Indeed, in the ACC silicon uptake is well described using the Michaelis-Menten relationship (Pondaven et al., 1998, 2000). The integrated (mixed layer depth = MLD) gross $bSiO_2$ production (P; mmol m^{-2} d^{-1}) is described as follows:

$$P = \int_0^{MLD} V_{Si[t]} \cdot [bSiO_2^{ML}]_{[t]} \cdot dz \quad (7)$$

The "ML" superscript indicates mixed layer biogenic silica (being the initial $bSiO_2$ + net $bSiO_2$ production, at each time step), which is a mixture of detrital and living diatom cells (Krause et al., 2010). The $bSiO_2$ export (= E) is described by a first order equation (first order constant = k_{export}):

$$E = \int_0^{MLD} k_{export} \cdot [bSiO_2^{ML}]_{[t]} \cdot dz \quad (8)$$

The $bSiO_2$ dissolution:production (D:P) ratio is assumed to increase linearly (from 0.0 to 1.0 over the expected range Brzezinski et al., 2003; Fig. 5d):

$$\frac{d\left(\frac{D}{P}\right)}{dt} = \frac{1}{N_{season}} \quad (9)$$

where N is the number of days. The model could be oversimplified as in the ACC, D:P ratios exceeding 1 have already been documented at the end of summer (Beucher et al., 2004; Fripiat et al., 2011c). This has been explained by an accumulation of detrital diatom cells in the mixed layer after a productive period.

The fractionation factor associated with Si-uptake, $^{30}\varepsilon_{upt}$, has been compiled for the ACC at -1.2 ± 0.2‰ in Fripiat et al. (2011b). Demarest et al. (2009) report that during dissolution of biogenic silica, light Si-isotopes are released preferentially ($^{30}\varepsilon_{diss} = -0.55$‰). This effect partly counteracts the fractionation occurring during $bSiO_2$ production. By increasing the mixed layer D:P ratio, the net fractionation ($^{30}\varepsilon_{net}$) factor associated with net $bSiO_2$ production (= net$P$) would be dampened as follows (Demarest et al., 2009):

$$^{30}\varepsilon_{net} = {}^{30}\varepsilon_{upt} + \frac{D}{P}.{}^{30}\varepsilon_{diss} \quad (10)$$

Therefore, assuming a D:P ratio evolution as described in Eq. (9), the $^{30}\varepsilon_{net}$ at the beginning of the productive period will be equal to the $^{30}\varepsilon_{upt}$ (-1.2‰) and decrease to -0.65‰($^{30}\varepsilon_{upt} - {}^{30}\varepsilon_{diss}$) at the end, in agreement with Eq. (10). In the following discussion, model results with and without an isotopic fractionation during $bSiO_2$ dissolution will be compared.

Using the above parameters and assuming the silicic acid pool is homogeneous and is fed with silicic acid of constant δ^{30}Si composition, the seasonal evolution can be described as follows:

$$\frac{d\left(m_{Si(OH)4}\right)}{dt} = F_{supply} + \left(\frac{D}{P}_{[t]} - 1\right) \cdot P_{[t]} = F_{supply} - \text{net}P_{[t]} \quad (11)$$

$$m_{Si(OH)4} . \frac{d\left(\delta^{30}Si_{Si(OH)4}\right)}{dt} = F_{supply} \cdot \delta^{30}Si_{supply} - {}^{30}\varepsilon_{[t]} \cdot \text{net}P_{[t]} \quad (12)$$

where m is the molar quantity of silicon (mmol m^{-2}) and F_{supply} the $Si(OH)_4$ supply (mmol m^{-2} d^{-1}).

The biogenic silica pools are described as follows:

$$\frac{d\left(m^{ML}_{bSiO2}\right)}{dt} = \text{net}P_{[t]} - E_{[t]} \quad (13)$$

$$m^{ML}_{bSiO2} . \frac{d\left(\delta^{30}Si^{ML}_{bSiO2}\right)}{dt} = \text{net}P_{[t]} \cdot \left(\delta^{30}Si_{Si(OH)4[t]} + {}^{30}\varepsilon_{[t]}\right) - E_{[t]} \cdot \delta^{30}Si^{ML}_{bSiO2[t]} \quad (14)$$

$$\frac{d\left(m^{export}_{bSiO2}\right)}{dt} = E_{[t]} \quad (15)$$

$$m^{export}_{bSiO2} . \frac{d\left(\delta^{30}Si^{export}_{bSiO2}\right)}{dt} = E_{[t]} \cdot \delta^{30}Si^{ML}_{bSiO2[t]} \quad (16)$$

Superscript "export" is the biogenic silica exported out of the mixed layer assuming that the exported fraction of biogenic silica has an isotopic composition similar to the one in the mixed layer. This could be an oversimplification since recently Krause et al. (2010) suggested that for the Equatorial Pacific exported biogenic silica can be composed of mainly detrital diatom cells.

Small errors arise for both mixing and fractionation when the δ notation is used instead of isotopic ratios. However, for δ values close to 0, as is the case for Si, these sources of errors are negligible (Fry, 2006). The aim here is to assess how the seasonal variability of the different isotopic effects potentially affects the mass and isotopic balances. This is of crucial importance for palaeoceanographic reconstructions of past ocean conditions. This approach should not be taken as an attempt to quantify fluxes (uptake, dissolution, export, and $Si(OH)_4$ supply). A more constrained model to solve the seasonal mass and isotopic balances, in a similar manner as for ^{30}Si-isotope dilution experiments (Elskens et al., 2007), is proposed by de Brauwere et al. (2011).

4.1.2 Model outputs

The model seems to adequately reproduce the seasonal evolution of silicic acid and biogenic silica concentrations in the PFZ mixed layer (Fig. 5b; Moore and Abbot, 2000; Quéguiner and Brzezinski, 2002). The integrated Si-uptake of 1.7 mol Si m^{-2} yr^{-1} fits relatively well with the mean expected values in the Polar Front Zone, 1.2 mol Si m^{-2} yr^{-1} (Fripiat et al., 2011c).

The simulated isotopic trends for $\delta^{30}Si_{bSiO2}$ differ from the $\delta^{30}Si_{Si(OH)4}$ trends, especially at the end of the productive period (Fig. 6a). In the PFZ the Si uptake over supply ratio is high at the beginning of the growth period and consequently the $\delta^{30}Si_{Si(OH)4}$ and $\delta^{30}Si_{bSiO2}$ evolutions roughly follow a Rayleigh-type evolution (Figs. 5d and 6c). Note that the steady state model is unable to reproduce the measured ML $\delta^{30}Si_{bSiO2}$ value and is in disagreement with the present simulation (Fig. 6d). Once the silicic acid concentration has reached a level that limits Si-uptake (Eq. 6), the Si uptake-over-supply ratio decreases and the supply by vertical mixing of light Si-isotopes into the Si-depleted mixed layer decreases $\delta^{30}Si_{Si(OH)4}$ (Figs. 5d and 6c). The $\delta^{30}Si_{bSiO2}$ is affected differently, since both new and preceding diatom generations set the ML $\delta^{30}Si_{bSiO2}$ (Eq. 14), especially at the end of the productive period when $bSiO_2$ production is low. Such process decrease the $\Delta^{30}Si$, as measured (Figs. 2b, 3, and 7a). The exported $bSiO_2$ out of the mixed layer fits with an accumulation product (sensu Rayleigh; Fig. 6c). This is seen from (1) Fig. 5b showing that the accumulated exported $bSiO_2$ is stable and is not significantly affected by processes occurring at the end of the productive period when the Si uptake:supply ratio is low, and (2) Fig. 7b showing the non-significant different relationship between the simulated exported $\delta^{30}Si_{bSiO2}$ and the accumulated biogenic silica (sensu Rayleigh) with relative silicon utilisation ($=f$). Note that this simulation is already able to explain, at least in part, the high and low measured $\Delta^{30}Si$ (Figs. 3 and 7a).

Impact of isotopic fractionation during dissolution: By adding the isotopic fractionation of $bSiO_2$ dissolution (Demarest et al., 2009), the $\delta^{30}Si_{Si(OH)4}$ is getting lighter and the $\delta^{30}Si_{bSiO2}$ heavier (Fig. 6a) throughout with the productive period, in agreement with a decrease in the net fractionation extent (Eq. 10). This process together with the low Si-uptake:supply ratio could explain the extremely low measured $\Delta^{30}Si$ at the end of the productive period (Fig. 7a). The latter could bias the relationship between the exported $\delta^{30}Si_{bSiO2}$ and the relative silicic acid utilization ($=f$). Nevertheless, such bias is lying within isotopic analytical precision (Fig. 7b) and should therefore have no impact on the utilization and interpretation of this proxy in palaeoceanography. Furthermore, the dissolution isotopic effect could have been over-expressed in this simulation since the D:P ratio at the $bSiO_2$ productive peak was already high (0.4) in comparison with published values (closer to 0.1; Brzezinski et al., 2003).

Impact of mixing events: By switching from a continuous supply to a pulsed supply mode, consisting of 10 consecutive instantaneous mixing events, the simulation is scattered around the continuous supply with no effect on biogenic silica isotopic composition (Fig. 6b). Moreover, in reality, mixing is probably spatially heterogeneous and lateral mixing should smooth the trends toward the mean continuous supply.

As a comparison, similar simulations have been carried out in the SAZ an area characterized, in contrast to PFZ, by a low vertical silicic acid gradient, and in the AZ characterized by a partly Si-depleted summer mixed layer (Fripiat et al., 2011a). In order to agree as much as possible with the PFZ simulation, the Si-supply over $bSiO_2$ production ratio has been fit at ∼0.3 and the D:P ratio at the productive peak at ∼0.4. For the same relative vertical mixing, the vertical supply of light Si-isotopes at the end of summer (low Si-uptake:supply ratio) is not sufficient to decrease the mixed layer $\delta^{30}Si_{Si(OH)4}$ (Fig. 8). Therefore it enables us to explain low $\Delta^{30}Si$ values observed only in the PFZ and PF (Fig. 2b), both characterized by heavily Si-depleted mixed layer

together with a large vertical silicic acid gradient.

The relationship between the accumulated exported $\delta^{30}Si_{bSiO2}$ and relative Si-utilization was not significantly different from the simulation with the accumulated product (sensu Rayleigh; Fig. 7b), both with and without isotopic fractionation during $bSiO_2$ dissolution. Therefore for reconstructing past $Si(OH)_4$ utilisation in the ACC surface waters from sedimentary $\delta^{30}Si_{bSiO2}$ data, our results indicate that a Rayleigh $bSiO_2$ accumulated product model is more appropriate than a steady state model. This mainly results from the high silicic acid supply:consumption ratio during the major part of the $bSiO_2$ production period and as a result the mixing effect has no significant impact on the exported $\delta^{30}Si_{bSiO2}$.

4.2 Fate of biogenic silica isotopic composition across the water column

The fate of biogenic silica $\delta^{30}Si$ through the water column is of prime importance to link the sedimentary $\delta^{30}Si$ to the environmental conditions in which they were generated. Dissolution during settling could affect the $\delta^{30}Si_{bSiO2}$ distributions by shifting the preserved material toward more positive values (Demarest et al., 2009). We present the first whole water column profiles of suspended biogenic silica $\delta^{30}Si$ signatures (Fig. 4). By analysing the $\delta^{30}Si$ of sinking biogenic silica (two sediment traps in the AZ at 1031 and 2182 m in the Pacific sector; Varela et al., 2004) a remarkable agreement with surface values was observed, which also paralleled the seasonal cycle of surface $bSiO_2$ production. This is further confirmed by the present study, since the isotopic composition of subsurface suspended biogenic silica reflects that of the mixed layer (Fig. 4). It thus seems that dissolution does not significantly affect the $\delta^{30}Si$ signal of exported $bSiO_2$. However, there are two exceptions:

1. In the WG, the $\delta^{30}Si_{bSiO2}$ is becoming heavier by 0.4 to 0.8 ‰ below 1800 m (Fig. 4). Since no values are available between 700 and 1800 m we do not know whether this shift is progressive or occurs only at a specific depth range. Cavagna et al. (2011a), observed that the $\delta^{13}C$ composition of deep ocean particles during

BGH is consistent mostly with a 1-D vertical transport and therefore it cannot be ruled out as a progressive dissolution of biogenic silica, preferentially releasing light silicon isotopes.

2. The strong $\delta^{30}Si_{bSiO2}$ lightening, by 0.6 ‰, below the mixed layer in the WG might result from biogenic silica produced from a subsurface $Si(OH)_4$ pool with lower $\delta^{30}Si_{Si(OH)4}$ as is present at such depths (Table 1; Fripiat et al., 2011a). Indeed, these depths extend below the euphotic layer (1 % PAR) and several studies have shown that energy involved in the silicification process is mainly of respiratory origin and therefore decoupled from photosynthesis (Martin-Jézéquel et al., 2000) allowing Si-uptake below the euphotic layer (Brzezinski et al., 1989).

5 Conclusions

Within a palaeoceanography perspective this study has attempted to assess the controls upon, and the seasonal evolution of, biogenic silica isotopic compositions in the mixed layer and its transfer across the water column. This data set acquired in late austral summer highlights two main points:

1. A large latitudinal variation in $\delta^{30}Si_{bSiO2}$ is observed in the mixed layer across the meridional BGH transect, contrasting with a narrower variation for $\delta^{30}Si_{Si(OH)4}$. This decoupling cannot be reproduced by Rayleigh and steady state isotopic fractionation models, which directly link the $\delta^{30}Si$ to relative $Si(OH)_4$ utilisation. These model failures probably result from the fact that (i) a constant isotopic fractionation is assumed over the entire period of silicate depletion and (ii) seasonal expression of the different isotopic effects is not taken into account (i.e. only Si-uptake is considered). We implemented an isotopic fractionation model to describe the seasonal $\delta^{30}Si$ variation in the mixed layer. From this analysis, it seems that the exported biogenic silica is rather well described by the Rayleigh accumulated product. The failures of the existing models are especially significant at the end of

the productive period when (i) biogenic silica production is low; (ii) $bSiO_2$ dissolution:production ratio is high, imposing a lower apparent fractionation factor and (iii) Si-supply:Si-uptake ratio is high. The latter effect is especially expressed when the summer mixed layer is strongly Si-depleted and a large silicic acid gradient has formed, as is the case in the southern ACC.

2. Except below 1800 m in the Weddell Gyre, where we cannot rule out a potential $bSiO_2$ dissolution effect, the deeper $\delta^{30}Si_{bSiO2}$ is generally similar to the mixed layer $\delta^{30}Si_{bSiO2}$, which supports the absence of an isotopic effect during particle settling through the water column in most cases.

Acknowledgements. Our warm thanks go to the officers and crew of the R/V *Marion Dufresne* during the BONUS-Goodhope cruise, as well as to S. Speich and M. Boyé as program leaders. We are also grateful to J. De Jong and N. Mattielli for the management of the MC-ICP-MS laboratory at ULB and to L. Monin and N. Dahkani (RMCA) for their help in sample processing and to Virginia Panizzo (ULB) for correction of English. This work was conducted within the BEL-CANTO III network (contracts SD/CA/03A of SPSDIII, Support Plan for Sustainable Development) funded by BELSPO, the Belgian Science Policy. Luc André thanks the "Fonds National de la Recherche Scientifique" (FNRS, Belgium) for its financial support (FRFC project 2.4512.00). François Fripiat and Anouk de Brauwere are post-doctoral fellows with the FNRS.

References

Abraham, K., Opfergelt, S., Fripiat, F., Cavagna, A.-J., de Jong, J. T. M., Foley, S. F., André, L., and Cardinal, D.: δ^{30}Si and δ^{29}Si determinations on USGS BHVO-1 and BHVO-2 reference materials with a new configuration on a Nu Plasma Multi-Collector ICP-MS, Geost. Geoanal. Res., 32, 193–202, 2008.

Allison, D. B., Stramski, D., and Mitchell, B. G.: Seasonal and interannual variability of particulate organic carbon within the Southern Ocean from satellite ocean color observations, J. Geophys. Res., 115, C06002, doi:10.1029/2009JC005347, 2010.

Anderson, R. F., Chase, Z., Fleisher, M. Q., and Sachs, J.: The Southern Ocean's biological pump during the Last Glacial Maximum, Deep-Sea Res. II, 49, 1909–1938, 2002.

Anderson, R. F., Ali, S., Bradtmiller, L. I., Nielsen, S. H. H., Fleisher, M. Q., Anderson, B. E., and Burckle, L. H.: Wind-driven upwelling in the Southern Ocean and the deglacial rise in atmmospheric CO_2, Science, 323, 1443–1448, doi:10.1126/science.1167441, 2009.

Beucher, C., Tréguer, P., Hapette, A.-M., and Corvaisier, R.: Intense summer Si-recycling in the surface Southern Ocean, Geophys. Res. Lett., 31, L09305, doi:10.1029/2003GL018998, 2004.

Beucher, C. P., Brzezinski, M. A., and Crosta, X.: Silicic acid dynamics in the glacial sub-Antarctic: Implications for the silicic acid leakage hypothesis, Global Biogeochem. Cycles, 21, GB3015, doi:10.1029/2006GB002746, 2007.

Brzezinski, M. A. and Nelson, D. M.: Seasonal changes in the silicon cycle within a Gulf Stream warm-core ring, Deep-Sea Res., 36, 1009–1030, 1989.

Brzezinski, M. A., Nelson, D. M, Franck, V. M., and Sigmon, D. E.: Silicon dynamics within an intense open-ocean diatom bloom in the Pacific sector of the Southern Ocean, Deep-Sea Res. II, 48, 3997–4018, 2001.

Brzezinski, M. A., Pride, C. J., Franck, V. M., Sigman, D. M., Sarmiento, J. L., Matsumoto, K., Gruber, N., Rau, G. H., and Coale, K. H.: A switch from $Si(OH)_4$ to NO_3^- depletion in the glacial Southern Ocean, Geophys. Res. Lett., 29, 1564, doi:10.1029/2001GL014349, 2002.

Brzezinski, M. A., Jones, J. L., Bidle, K. D., and Azam, F.: The balance between silica production and silica dissolution in the sea: Insights from Monteray Bay, California, applied to the global data set, Limnol. Oceanogr., 48, 1846–1854, 2003.

Cardinal, D., Alleman, L. Y., de Jong, J., Ziegler, K., and André, L.: Isotopic composition of silicon measured by multicollector plasma source mass spectrometry in dry plasma mode, J. Anal. Atom. Spectrom., 18, 213–218, 2003.

Cardinal, D., Alleman, L. Y., Dehairs, F., Savoye, N., Trull, T. W., and André, L.: Relevance of silicon isotopes to Si-nutrient utilization and Si-source assessment in Antarctic waters, Global Biogeochem. Cycles, 19, GB2007, doi:10.1029/2004GB002364, 2005.

Cardinal, D., Savoye, N., Trull, T. W., Dehairs, F., Kopczynska, E. E., Fripiat, F., Tison, J.-L., and André, L.: Silicon isotopes in spring Southern Ocean diatoms: large zonal changes despite homogeneity among size fractions, Mar. Chem., 106, 46–62, 2007.

Cavagna, A.-J., Dehairs, F., Woule-Ebongué, V., Delille, B., and Bouloubassi, I.: Whole water column distribution and carbon isotopic composition of cholesterol and brassicasterol from the Cape Basin to the northern Weddell Gyre, Biogeosciences Discuss., in preparation, 2011a.

Cavagna, A.-J., Fripiat, F., Dehairs, F., Wolf-Gladrow, D., Cisewski, B., Savoye, N., André, L., and Cardinal, D.: Silicon uptake and supply during a Southern Ocean iron fertilization experiment (EIFEX) tracked by Si isotopes, Limnol. Oceanogr., 56, 147–160, 2011b.

de Brauwere, A., Fripiat, F., Cardinal, D., Cavagna, F., Dehairs, A.-J., André, L., and Elskens, M.: Isotopic model of oceanic silicon cycling: the Kerguelen Plateau case study, Global Biogeochem. Cycles, in preparation, 2011.

De La Rocha, C. L.: Opal-based isotopic proxies of paleoenvironmental conditions, Global Biogeochem. Cycles, 20, GB4S09, doi:10.1029/2005GB002664, 2006.

De La Rocha, C. L., Brzezinski, M. A., and DeNiro, M. J.: Purificaiton recovery and laser-driven fluorination of silicon from dissolved and particulate silica for the measurement of natural stable isotope abundances, Anal. Chem., 68, 3746–3750, 1996.

De La Rocha, C. L., Brzezinski, M. A., and DeNiro, M. J.: Fractionation of silicon isotopes by marine diatoms during biogenic silica formation, Geochim. Cosmochim. Acta, 61, 5051–5056, 1997.

De La Rocha, C. L., Brzezinski, M. A., and DeNiro, M. J.: Silicon-isotope composition of diatoms as an indicator of past oceanic change, Nature, 395, 680–683, 1998.

Demarest, M. S., and Brzezinski, M. A., and Beucher, C. P.: Fractionation of silicon isotopes during biogenic silica dissolution, Geochim. Cosmochim. Acta, 73, 5572–5583, doi:10.1016/j.gca.2009.06.019, 2009.

Douthitt, C. B.: The geochemistry of the stable isotopes of silicon, Geochim. Cosmochim. Acta, 46, 1449–1458, 1982.

Elskens, M., de Brauwere, A., Beucher, C., Corvaisier, R., Savoye, N., Tréguer, P., and Baeyens, W.: Statistical process control in assessing production and dissolution rates of biogenic silica in marine environments, Mar. Chem., 106, 272–286, 2007.

Fripiat, F.: Isotopic approaches of the silicon cycles: The Southern Ocean case study, Ph.D. thesis, Université Libre de Bruxelles, available at http://theses.ulb.ac.be/ETD-db/collection/available/ULBetd-12142009-190405/, 2010.

Fripiat, F., Cavagna, A.-J., Dehairs, F., Speich, S., André, L., and Cardinal, D.: Silicon pool dynamics and biogenic silica export in the Southern Ocean inferred from Si-isotopes, Ocean Sci., 7, 533–547, doi:10.5194/os-7-533-2011, 2011a.

Fripiat, F., Cavagna, A.-J., Savoye, N., Dehairs, F., André, L., and Cardinal, D.: Isotopic constraints on the Si-biogeochemical cycle of the Antarctic Zone in the Kerguelen area (KEOPS), Mar. Chem., 123, 11–22, 2011b.

Fripiat, F., Leblanc, K., Elskens, M., Cavagna, A.-J., Armand, L., André, L., Dehairs, F., and Cardinal, D.: Summer efficient silicon loop across the Polar Front and Sub-Antarctic Zones despite contrasted diatom Si-affinity, Mar. Ecol. Prog. Ser., 435, 47–61, doi:10.3354/meps09237, 2011c.

Fry, B.: Stable Isotope Ecology, Springer, New York, pp. 308, 2003.

Fütterer, D. K.: The solid phase of marine sediments, in: Marine Geochemistry, Springer, New York, 1–25, doi:10.1007/3-540-32144-6_1, 2006.

Georg, R. B., Zhu, C., Reynolds, B. C., and Halliday, A. N.: Stable silicon isotopes of groundwater, feldspars, and clay coating in the Navajo Sandstone aquifer, Black Mesa, Arizona, USA, Geochim. Cosmochim. Acta, 73, 2229–2241, 2009b.

Grasshof, K., Erhardt, M., and Kremling, K.: Methods of seawater analysis, 2nd ed. Verlag Chemie, Weinheim, 1983.

Karl, D. M. and Tien, G.: MAGIC: a sensitive and precise method for measuring dissolved phosphorus in aquatic environments, Limnol. Oceanogr., 37, 105–116, 1992.

Krause, J. W., Brzezinski, M. A., Landry, M. R., Baines, S. B., Nelson, D. M., Selph, K. E., Taylor, A. G., and Twining, B. S.: The effects of biogenic silica detritus, zooplankton grazing, and diatom size structure on silicon cycling in the euphotic zone of the eastern equatorial Pacific, Limnol. Oceanogr., 55, 2608–2622, 2010.

Martin-Jézéquel, V., Hildebrand, M., and Brzezinski, M. A.: Review: Silicon metabolism in diatoms: implications for growth, J. Phycol., 36, 821–840, 2000.

Mongin, M., Matear, R., and Chamberlain, M.: Seasonal and spatial variability of remotely sensed chl and physical fields in the SAZ-Sense region, Deep-Sea Res. II, 58, 2082–2093, 2011.

Moore, J. K. and Abbott, M. R.: Phytoplankton chlorophyll distributions and primary production in the Southern Ocean, J. Geophys. Res., 106, 28709–28722, 2000.

Opfergelt, S., Cardinal, D., André, L., Delvigne, C., Bremond, L., and Delvaux, B.: Variations of δ^{30}Si and Ge/Si with weathering and biogenic input in tropical basaltic ash soils under monoculture, Geochim. Cosmochim. Acta, 74, 225–240, 2010.

Pondaven, P., Fravalo, C., Ruiz-Pino, D., Tréguer, P., Quéquiner, B., and Jeandel, C.: Modelling the silica pump in the Permanently Open Ocean Zone of the Southern Ocean, J. Mar. Syst., 17, 578–619, 1998.

Pondaven, P., Ruiz-Pino, D., Fravalo, C., Tréguer, P., and Jeandel, C.: Interannual variability of Si and N cycles at the time-series station KERFIX between 1990 and 1995 – a 1-D modelling

study, Deep Sea Res. I, 47, 223–257, 2000.
Quéguiner, B. and Brzezinski, M. A.: Biogenic silica production rates and particulate matter distribution in the Atlantic sector of the Southern Ocean During austral spring 1992, Deep-Sea Res., 49, 1765–1786, 2002.
Ragueneau, O., Savoye, N., Del Amo, Y., Cotten, J., Tardiveau, B., and Leynaert, A.: A new method for the measurement of biogenic silica in suspended matter of coastal waters : using Si :Al ratios to correct for the mineral interference, Cont. Shelf Res., 25, 697–710, 2005.
Reynolds, B. C., Frank, M., and Halliday, A. N.: Silicon isotope fractionation during nutrient utilization in the North Pacific, Earth Planet. Sci. Lett., 244, 431–443, 2006.
Reynolds, B. C., Aggarwal, J., André, L., Baxter, D., Beucher, C., Brzezinski, M. A., Engström, E., Georg, R. B., Land, M., Leng, M. J., Opfergelt, S., Rodushkin, I., Sloane, H. J., van den Boorn, H. J. M., Vroon, P. Z., and Cardinal, D.: An inter-laboratory comparison of Si isotope reference materials, J. Anal. Atom. Spectrom., 22, 561–568, doi:10.1039/b616755a, 2007.
Sarmiento, J. L., Gruber, N., Brzezinski, M. A., and Dunne, J. P.: High-latitude controls of thermocline nutrients and low latitude biological productivity, Nature, 427, 56–60, 2004.
Sigman, D. M., Hain, M. P., and Haug, G. H.: The polar ocean and glacial cycles in atmospheric CO_2 concentration, Nature, 466, 47–55, doi:10.1038/nature09149, 2010.
Taylor, S. R. and McLennan, S. M.: The continental crust: its composition an devolution, Blackwell Scientific Publications, Oxford, pp. 312, 1985.
Varela, D. E., Pride, C. J., and Brzezinski, M. A.: Biological fractionation of silicon isotopes in Southern Ocean surface waters, Global Biogeochem. Cycles, 18, GB1047, doi:10.1029/2003GB002140, 2004.
Ziegler, K., Chadwick, O. A., Brzezinski, M. A., and Kelly, E. F.: Natural variations of δ^{30}Si ratios during progressive basalt weathering, Hawaiian Islands, Geochim. Cosmochim. Acta, 69, 4597–4610, 2005.

Table 1. $Si(OH)_4$ and $bSiO_2$ concentrations and isotopic compositions. Only the standard deviations for duplicates are shown. Bold numbers represent samples from in situ pump.

Station	Depth m	$Si(OH)_4$ µmol l^{-1}	$\delta^{30}Si_{Si(OH)4}$ ‰ ± sd	Depth m	$bSiO_2$ µmol l^{-1}	$\delta^{30}Si_{bSiO2}$ ‰ ± sd
Super 5	29	65.2	1.85 ± 0.03	**30**	**0.36**	**0.28 ± 0.04**
16 March 2008	88	64.2	2.00	88	1.23	0.28
00.02° E–57.32° S	151	84.1	1.50 ± 0.03	**140**	**0.12**	**−0.40 ± 0.10**
	199	96.2	1.35 ± 0.01	**250**	**0.23**	**0.16 ± 0.01**
	251	101.5	1.37 ± 0.05	**400**	**0.18**	**0.27 ± 0.03**
	299	104.2	1.41 ± 0.05	**700**	**0.10**	**0.26 ± 0.02**
	400	110.5	1.44 ± 0.36	**1800**	**0.05**	**0.68 ± 0.11**
	499	117.2	1.47	**2500**	**0.04**	**0.65 ± 0.15**
	700	116.5	1.44 ± 0.20	**3200**	**0.04**	**0.72 ± 0.12**
	1003	120.0	1.27	**3874**	**0.03**	**0.92 ± 0.08**
	1499	119.1	1.13			
	1999	116.6	1.12 ± 0.06			
	2500	119.7	1.43			
	3000	117.2	1.11 ± 0.08			
	3979	118.8	1.08			
Large 7	4	50.7	1.95	4	0.40	0.42 ± 0.11
14 March 2008	39	n.a.	n.a.	39	0.72	0.53 ± 0.04
00.03° E–55.14° S	80	50.0	1.78 ± 0.07	80	0.38	0.50
Super 4	11	22.2	2.42	11	0.31	1.38
11 March 2008	41	n.a.	n.a.	41	0.39	1.28
0.00° E–51.87° S	60	n.a.	n.a.	**60**	**0.30**	**1.37 ± 0.10**
	79	22.3	2.37 ± 0.06	79	0.29	1.18
	100	21.9	2.16 ± 0.08	100	n.a.	n.a.
	149	30.5	2.03	**170**	**0.37**	**1.41 ± 0.06**
	199	63.2	1.48 ± 0.00	**260**	**0.28**	**1.36 ± 0.06**

Table 1. Continued.

Station	Depth m	$Si(OH)_4$ µmol l^{-1}	$\delta^{30}Si_{Si(OH)4}$ ‰ ± sd	Depth m	$bSiO_2$ µmol l^{-1}	$\delta^{30}Si_{bSiO2}$ ‰ ± sd
	300	86.0	1.41 ± 0.09	**420**	**0.14**	**1.34 ± 0.21**
	398	87.6	1.58	**749**	**0.13**	**1.32 ± 0.10**
	553	88.9	1.37 ± 0.16	**1128**	**0.14**	**1.30 ± 0.18**
	704	90.1	1.53	**1695**	**0.03**	**1.24 ± 0.15**
	1201	101.9	1.35	**2488**	**0.11**	**1.42 ± 0.20**
	1601	109.5	1.47			
	2001	121.7	1.30			
	2551	131.2	1.13			
Large 6	3	4.0	2.47	3	0.13	
8 March 2008	48	4.0	2.48	48	0.31	2.00 ± 0.02[a]
01.18° E–50.22° S	98	5.1	2.47	98	0.32	
Super 3	5	2.1	3.24 ± 0.01	5	0.13	
6 March 2008	41	2.2	2.85	41	0.32	2.50 ± 0.06[a]
4.23° E–47.33° S	79	2.2	2.36	79	0.06	
	100	4.2	2.57 ± 0.19	100	0.10	
	149	9.2	2.30	**600**	**0.10**	**2.30 ± 0.03**
	200	10.4	2.42	**1068**	**0.05**	**2.29 ± 0.06**
	401	25.3	1.93 ± 0.35			
	600	42.5	1.67			
	1002	67.8	1.43			
Super 2	10	0.6	3.24	**70**	**0.04**	**2.03 ± 0.18**
27 February 2008	40	1.0	n.a.			
8.56° E–42.28° S						
Super 1	4	2.2	3.04 ± 0.24	4	0.08	
21 February 2008	25	2.3	2.89 ± 0.07	25	0.28	1.30 ± 0.10[a]
13.10° E–36.45° S	50	n.a.	n.a.	50	0.22	

[a] Samples in the mixed layer have been merged for Si-isotopic analysis

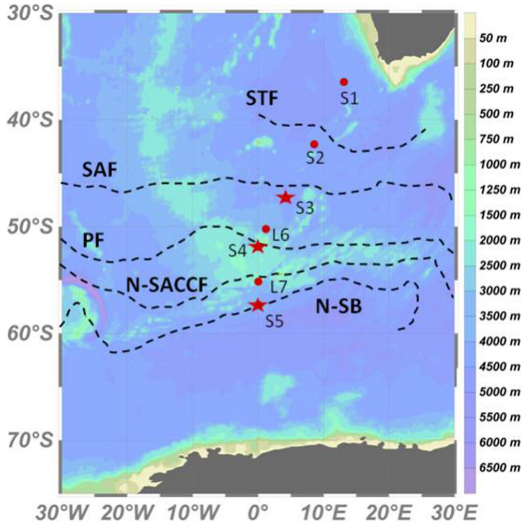

Fig. 1. Map of the study area with bathymetry and fronts (following Sokolov and Rintoul, 2009, and Swart et al., 2008): STF = SubTropical Front; SAF = SubAntarctic Front (middle branch); PF = Polar Front (middle branch); N-SACCF = northern branch of the Southern ACC front; N-SB = northern branch of the Southern Boundary (SB). The area north of the STF is the Sub-Tropical Zone (STZ); between STF and SAF the SubAntarctic Zone (SAZ); between the SAF and PF the Polar Front Zone (PFZ); between the PF and SB the Antarctic Zone (AZ), and south of the SB the northern part of the Weddell Gyre (WG). The stations where only the mixed layer was sampled are represented by dots. The stations where water column $bSiO_2$ samples have been collected are represented by the stars. S refers to "super" stations and L to "large" stations.

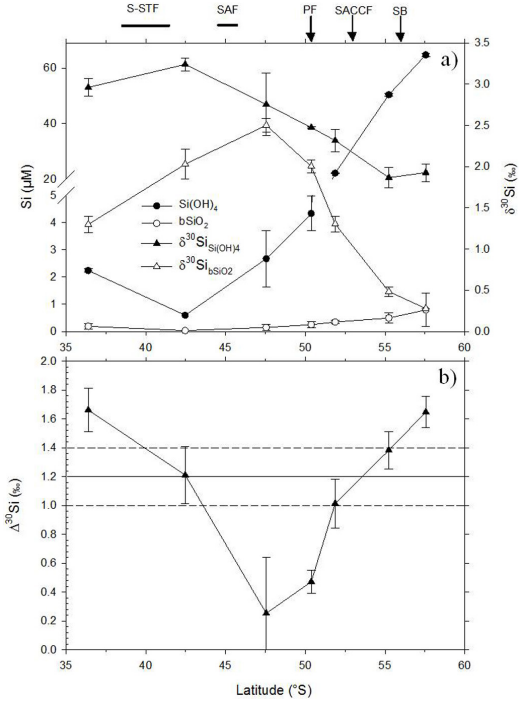

Fig. 2. **(a)** Latitudinal variation in the mixed layer (mean ± sd) for concentrations and isotopic composition. The dots represent the concentration and the triangles the isotopic compositions, respectively black and white for $Si(OH)_4$ and $bSiO_2$. Panel **(b)** shows the latitudinal variation of apparent fractionation factor ($\Delta^{30}Si = \delta^{30}Si_{Si(OH)4} - \delta^{30}Si_{bSiO2}$). The horizontal lines represent the compiled average ACC fractionation factor (−1.2 ± 0.2 ‰) given in Fripiat et al. (2011b). Arrows and lines represent the positions of the front at the time of sampling.

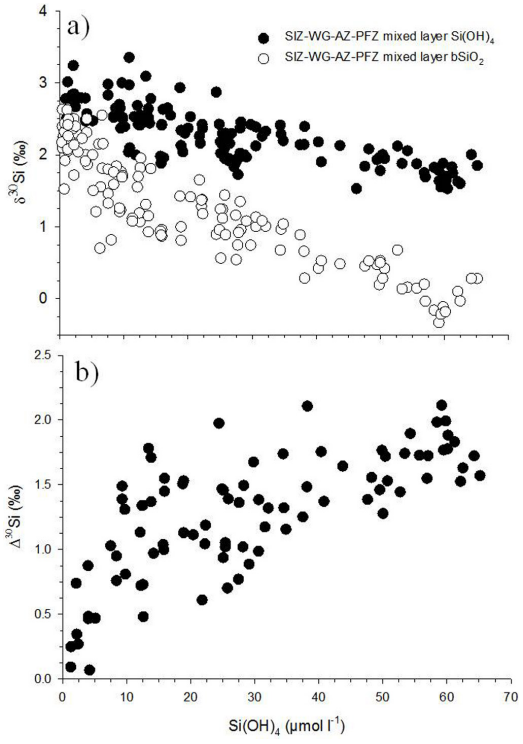

Fig. 3. **(a)** Mixed layer $\delta^{30}Si$ (both for $Si(OH)_4$ and $bSiO_2$) vs. $[Si(OH)_4]$ for the SIZ-WG, AZ, and PFZ. **(b)** Mixed layer $\Delta^{30}Si$ vs. $[Si(OH)_4]$ for the SIZ-WG, AZ, and PFZ (data from BGH: this study; AESOPS and SOFEX: Varela et al., 2004; CLIVAR-SR3: Cardinal et al., 2005, 2007; KEOPS: Fripiat et al., 2011b; EIFEX: Cavagna et al., 2011b).

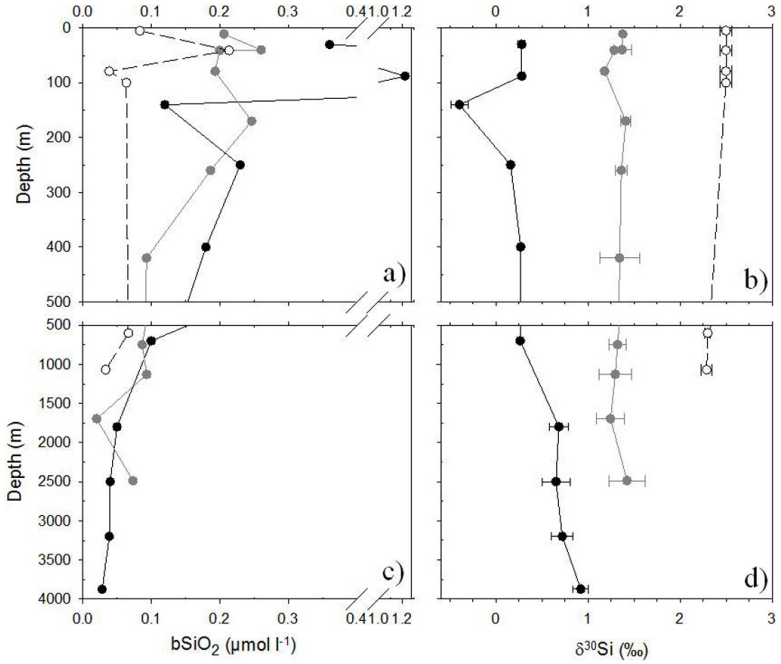

Fig. 4. Vertical profiles for the stations in the Weddell Gyre (filled black circles), the Antarctic Zone (filled gray circles), and the Polar Front Zone (empty black circles), respectively super 5, super 4 and super 3. **(a)** and **(c)** $bSiO_2$ concentration profiles. **(b)** and **(d)** $\delta^{30}Si$ profiles of $bSiO_2$.

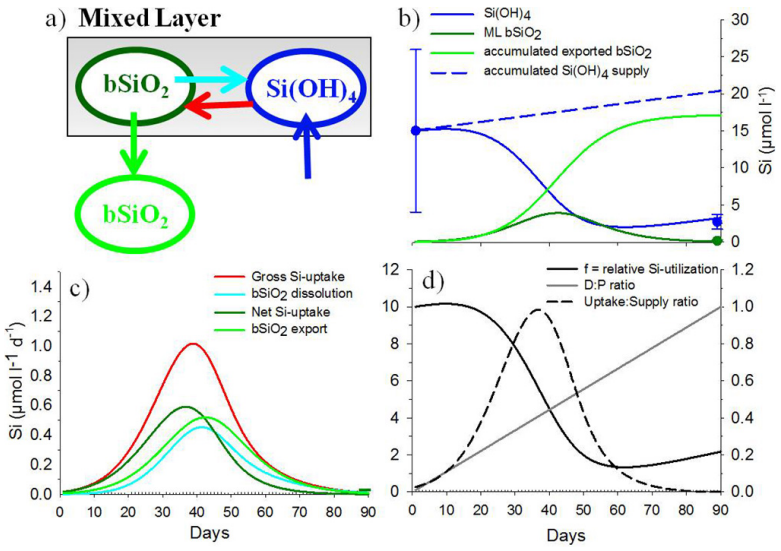

Fig. 5. **(a)** Schematic representation of the box model (= 100 m deep mixed layer). Round boxes represent pools of silicic acid in the mixed layer (blue), biogenic silica in the mixed layer (dark green), and accumulated exported biogenic silica below the mixed layer (light green). Arrows stand for processes exchanging Si between the pools: gross Si-uptake (red arrow), $bSiO_2$ dissolution (cyan arrow), $bSiO_2$ export (green arrow), and vertical $Si(OH)_4$ supply (blue arrow). **(b)**, **(c)**, **(d)** Model outputs for the PFZ simulation. **(b)** Simulated concentrations of $Si(OH)_4$ and $bSiO_2$ in the mixed layer, accumulated exported $bSiO_2$, and accumulated Si-supply to the mixed layer. **(c)** Simulated gross Si-uptake, $bSiO_2$ dissolution, net Si-uptake, and $bSiO_2$ export. **(d)** Simulated Si-uptake:supply ratio (left Y-axis), relative $Si(OH)_4$ utilization (f) and D:P ratio (right Y-axis). $V_{max} = 0.42$, $K_{Si} = 4\,\mu mol\,l^{-1}$, $k_{export} = 0.13$, and subsurface $Si(OH)_4$ supply = $540\,mmol\,m^{-2}$.

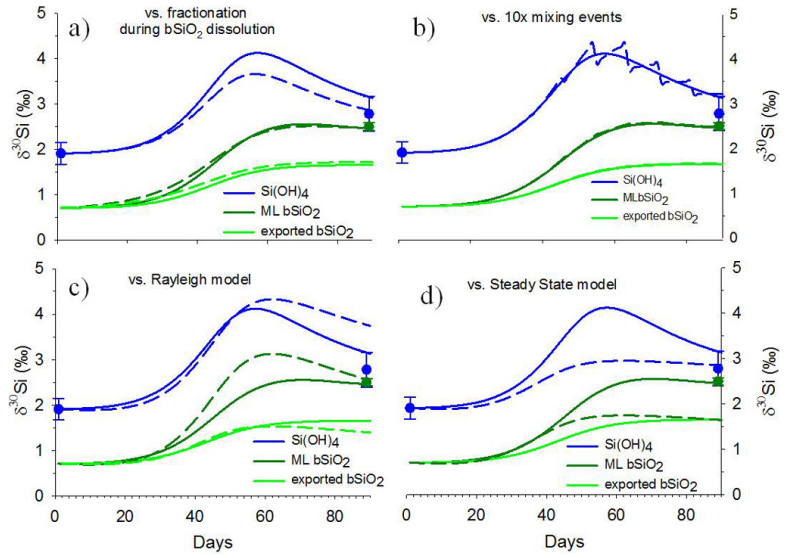

Fig. 6. Model outputs for the case study station in the PFZ. **(a)** Simulated δ^{30}Si values for $Si(OH)_4$, ML $bSiO_2$, exported $bSiO_2$ without (full lines) and with (dashed lines) $bSiO_2$ dissolution isotopic fractionation ($^{30}\varepsilon = -0.55$ ‰). **(b)** Simulated δ^{30}Si values for $Si(OH)_4$, ML $bSiO_2$, exported $bSiO_2$ with continuous Si-supply (full lines) and 10 mixing events (dashed lines). **(c)** Comparison between the simulated δ^{30}Si values (full lines) and Rayleigh model outputs (dashed line). For the Rayleigh model, ML $bSiO_2$ is the instantaneous product (sensu Rayleigh) and exported $bSiO_2$ the accumulated product (sensu Rayleigh). **(d)** Comparison between the simulated δ^{30}Si values (full lines) and the Steady State model outputs (dashed lines).

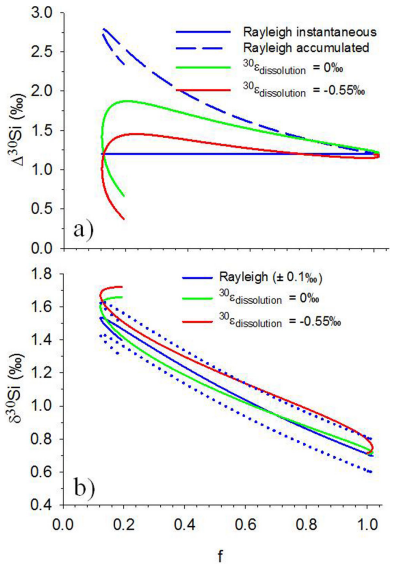

Fig. 7. (a) Simulated Δ^{30}Si (= $\delta^{30}Si_{Si(OH)4}$ – mixed layer $\delta^{30}Si_{bSiO2}$) vs. relative Si-utilisation in the mixed layer (= $[Si(OH)_4]_{(t)}$:$[Si(OH)_4]_{(t0)}$) without (green line) and with (red line) an isotopic fractionation during $bSiO_2$ dissolution. The isotopic difference between the Rayleigh $\delta^{30}Si_{Si(OH)4}$ and either Rayleigh instantaneous $\delta^{30}Si_{bSiO2}$ (full blue line) or Rayleigh accumulated $\delta^{30}Si_{bSiO2}$ (dashed blue line) are also shown. **(b)** Simulated relationship between accumulated exported $\delta^{30}Si_{bSiO2}$ and relative Si-utilization in the mixed layer without (green line) and with (red line) an isotopic fractionation during $bSiO_2$ dissolution. The relationship with the Rayleigh accumulated $\delta^{30}Si_{bSiO2}$ (full blue line; 1 standard deviation = dashed blue lines) is also shown to compare.

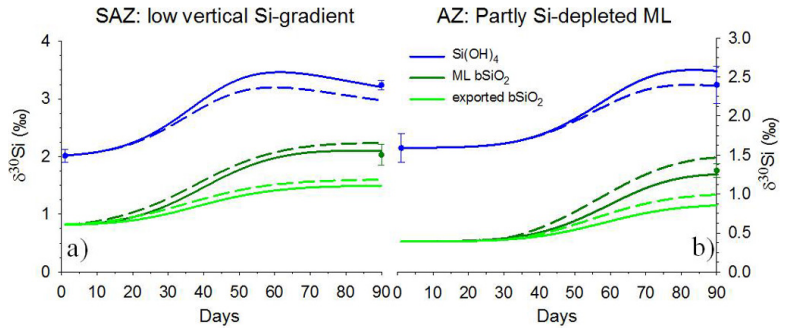

Fig. 8. Model outputs for the SAZ **(a)** and AZ **(b)**. Simulated δ^{30}Si values for $Si(OH)_4$, ML $bSiO_2$, exported $bSiO_2$ without (full lines) and with (dashed lines) $bSiO_2$ dissolution isotopic fractionation ($^{30}\varepsilon = -0.55$ ‰). Respectively for the SAZ and AZ: $V_{max} = 0.40$ and $0.31\ d^{-1}$, $K_{Si} = 2.2$ and $10\ \mu mol\ l^{-1}$, $k_{export} = 0.11$ and $0.13\ d^{-1}$, $Si(OH)_4$ supply = 108 and 1170 mmol m^{-2}, and net $bSiO_2$ production = 321 and 4054 mmol m^{-2}.